Institute for Advanced Technology
The University of Texas at Austin

IAT

Investigation of Oblique Penetration I: The Effects of Penetrator Leading End Shapes on Unyawed and Yawed Impacts

J. A. Hawkins, S. J. Bless, and M. Normandia

Institute for Advanced Technology
The University of Texas at Austin

March 1998

IAT.R 0144

REPORT DOCUMENTATION PAGE

Form Approved
OMB NO. 0704-0188

1. AGENCY USE ONLY (Leave blank)	2. REPORT DATE	3. REPORT TYPE AND DATES COVERED
	March 1998	Technical Report

4. TITLE AND SUBTITLE

Investigation of Oblique Penetration I: The Effects of Penetrator Leading End Shapes on Unyawed and Yawed Impacts

5. FUNDING NUMBERS

Contract # DAAA21-93-C-0101

6. AUTHOR(S)

J. A. Hawkins, S. J. Bless, and M. Normandia

7. PERFORMING ORGANIZATION NAME(S) AND ADDRESS(ES)

Institute for Advanced Technology
The University of Texas at Austin
4030-2 W. Braker Lane, #200
Austin, TX 78759

8. PERFORMING ORGANIZATION REPORT NUMBER

IAT.R 0144

9. SPONSORING / MONITORING AGENCY NAME(S) AND ADDRESS(ES)

U.S. Army Research Laboratory
ATTN: AMSRL-WT-T
Aberdeen Proving Ground, MD 21005-5066

10. SPONSORING / MONITORING AGENCY REPORT NUMBER

11. SUPPLEMENTARY NOTES

The view, opinions and/or findings contained in this report are those of the author(s) and should not be considered as an official Department of the Army position, policy, or decision, unless so designated by other documentation.

12a. DISTRIBUTION / AVAILABILITY STATEMENT

Approved for public release; distribution unlimited.

12b. DISTRIBUTION CODE

A

13. ABSTRACT *(Maximum 200 words)*

This report investigates the effects of nose shapes on simple oblique and yawed oblique impacts. For simple oblique penetration there is a significant amount of rod tip erosion. Novel shaped noses can be designed which minimize the amount of mass lost in erosion and which create efficient craters sufficient to allow passage of the upstream portion of the rod. Gains brought about by novel rod tip designs are not as evident in the yawed oblique impact case as in the simple oblique impact case. The gains made in the axial direction are obscured somewhat by the additional loading due to slot formation. However, nose shapes seem to affect the degree and nature of this load and may provide a means of reducing the damage caused by slot formation.

14. SUBJECT TERMS

nose shapes, penetrator, oblique penetration, yaw

15. NUMBER OF PAGES

13

16. PRICE CODE

17. SECURITY CLASSIFICATION OF REPORT	18. SECURITY CLASSIFICATION OF THIS PAGE	19. SECURITY CLASSIFICATION OF ABSTRACT	20. LIMITATION OF ABSTRACT
Unclassified	Unclassified	Unclassified	UL

Contents

List of Figures and Table

Investigation of Oblique Penetration I: The Effects of Penetrator Leading End Shapes on Unyawed and Yawed Impacts

James A. Hawkins, Stephan J. Bless, and Michael J. Normandia

Introduction

A common observation noted in oblique impact problems is that the resulting crater appears larger than necessary to allow the passage of the undisturbed, upstream portion of the rod. The question naturally arises "can the rod shape be optimized such that a minimum amount of mass is consumed during crater formation"? To answer this question, we have executed a series of AUTODYN simulations designed to find rod tip (nose) shapes that create efficient craters with less mass. Although this work was motivated by observations of oblique impacts, we have investigated the use of this approach in yawed oblique impact problems.

The crater formed by yawed oblique penetration is characterized by a narrow slot adjoining the normally occurring, unyawed penetration crater. The slot-cutting process introduces a complication not found in unyawed oblique penetration. As a result, minimizing material erosion while maintaining crater size is not the only goal in penetrator design. In yawed problems the additional load due to slot cutting must be eliminated or minimized. This report describes some of the nose shapes we have investigated in both unyawed and yawed oblique impacts. We will begin by describing a typical oblique penetration problem, some possible alternative nose shapes, and the resulting craters. Then, we will use the same approach to investigate yawed oblique impacts.

To avoid confusion, it is valuable to define obliquity as yaw with vector equations:

$$\theta = \sin^{-1}\left[\operatorname{sgn}(\vec{V}\times\hat{n})\frac{|\vec{V}\times\hat{n}|}{|\vec{V}|}\right] \tag{1}$$

and yaw (pitch)

$$\alpha = \sin^{-1}\left[\operatorname{sgn}(\vec{V}\times\vec{L})\frac{|\vec{V}\times\vec{L}|}{|\vec{V}||\vec{L}|}\right] \tag{2}$$

Here $\vec{V}$, $\vec{L}$, and $\hat{n}$ are impact velocity, rod length, and outward tangent normal. Thus, $\theta > 0$ $\alpha > 0$ implies a rod that is pitched away from the target plate.

Oblique Penetration

In this section we describe, in general terms, some characterizing features of oblique penetration. Figure 1 shows a series of illustrations from a simple oblique impact problem as simulated by AUTODYN. The rod is considered long in the sense that the length to diameter ratio is high, while the plate is considered thin because its thickness is on the order of the rod diameter. Initial conditions and dimensions for the rod and plate are shown in the table shown in Figure 1(b). The panels in Figure 1(a) show the penetration process at representative intervals. The materials are described in Table 1.

When impact first occurs a splash is created in the target, the result of cavitating pressure brought about by impact (see first panel Figure 1(a)). The initial diameter of the crater is such that the side of the rod closest to the crater wall and upstream of the impact is undisturbed by the crater surface. The impact crater surface grows quasi-spherically while maintaining the distance between the rod sidewall and the crater wall (second panel Figure 1(a)). As the rod penetrates deeper into the crater, its tip surface overtakes the developing crater surface and thereafter the interface between the rod and target is nearly normal to the rod axis. The rod continues to penetrate that smaller portion of the crater creating a slightly deformed spherical surface, much like a balloon with a finger punching on one side (third panel Figure 1(a)). Finally, the rod and the original spherical crater punch through the backside of the plate (fourth panel of Figure 1(a)). The resulting crater is longer than it is narrow giving it an oval shape.

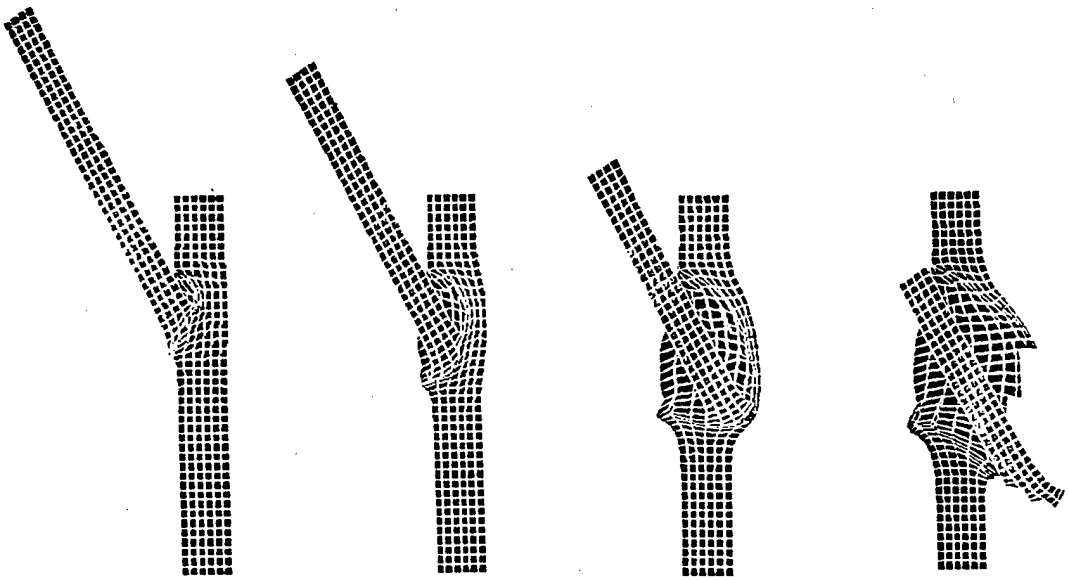

(a)

tungsten	L/D	10
rod	V(km/s)	2.6
RHA steel	T/D	1.2
plate	obliquity	60°

(b)

Fig. 1. Baseline oblique penetration problem: (a) four intervals during penetration and (b) associated input parameters.

Table I. Material properties (cm, g, μs) for AUTODYN simulation.

Material model/property	RHA steel plate	tungstsen rod
EOS	shock	shock
Strength	Von Mises	Von Mises
Failure	none	none
Erosion	geometric	geometric
Density (lg/cm^3)	7.86	17.4000
C1 ($cm/\mu s$)	0.461	00.4029
S1	1.730	01.2370
Grueisen coeff.	1.670	01.5400
Relative volume, VE	0.000	00.0000
Relative volume, VB	0.000	00.0000
C2 ($cm/\mu s$)	0.000	00.0000
S2	0.000	00.0000
Reference temp. (K°)	300	300
Specific heat (C.V.) (Terg/gK)	1.3×10^{-6}	1.34×10^{-6}
Shear modulus (Mbar)	0.8	1.45
Yield stress (Mbar)	9.6×10^{-3}	$2.0x10^{-2}$
Erosion strain	1.5	1.5

The exiting rod remnant is shorter with a slightly curled tip. The curl can be attributed to the rod tip's interaction with the lip of the exit crater. During penetration, the rod tip spreads slightly as the crater forms. On exiting, one part of the rod breaks through first, and the associated asymmetric load curls the tip toward the plate normal. Moreover, the rod's overall length has decreased as a result of erosion. While material erosion during high velocity penetration is a well known physical phenomenon, AUTODYN accounts for erosion by measuring the geometric distortion of individual cells and discarding those cells which exceed a prescribed amount of distortion. The amount of tolerable distortion is determined by the setting the geometric strain parameter (see Table 1). Before further discussion of the AUTODYN erosion results, we will discuss possible improvements in rod geometry.

Analysis of the crater dimensions suggests two penetrator geometries that are likely improvements to the baseline rod. First note that the major axis of the crater is significantly larger than the original rod diameter. Consequently, a follow-on rod of the same diameter as the tip has more room than necessary to clear the crater walls. This leads one to believe that a rod with a tapered small diameter tip could effectively penetrate the plate and minimize the mass lost to erosion. Alternatively, noting that initial crater formation is largely determined by the rod tip, a rod with a large (enough mass to create an efficient crater) leading tip or nose followed by a narrower rod portion or neck connecting to the bulk of the rod could act as a punch. The resulting pilot hole in the plate could be big enough to allow the main rod to pass relatively unhindered. While we have tried some tapered shapes, we have concentrated our efforts on punch shapes because of the increased savings in mass. The results have been encouraging, at least in the case of unyawed oblique impacts. Before discussing the application of nose shape design to oblique penetration problems we will discuss an experiment and a simulation that calibrate, to some extent, the computations discussed in this report.

Data comparison and mesh size effects

In this section we describe two experiments, one laboratory and one numerical, which are intended to check the range of validity for our simulations. First, an experiment was conducted during the preparation of this report which allowed comparison to the oblique penetration simulation shown in Figure 1. Second, a numerical simulation was conducted to investigate the effect of cell size, i. e., does an increase in cell size significantly change the results of the simulations? We first discuss a comparison of the penetration simulation results to experimental data.

The results of a recent oblique impact experiment (IAT shot #240), whose parameters were roughly the same as those in Figure 1(b), compare favorably to the results of the oblique impact simulation. An outline of the entrance crater[1] from experiment #240 is shown along with a front and side view of the AUTODYN calculated crater in Figure 2(a). The measurements from the tracing and recorded data were compared to the AUTODYN simulation discussed in the previous section. The comparison is shown in the table in Figure 2(b). The dimensions of the major and minor axes, D_{maj} and D_{min} respectively, of the crater have been

1. The tracing was made by placing a sheet of paper over the entrance crater and rubbing with a pencil.

normalized by the diameter of the rod, D_p. We have chosen to calculate only the dimensions of the entrance crater because the plate is thin and the dimensions of the exit crater are roughly the same. Erosion, the amount of penetrator used in the impact (as discussed above), has been normalized by the plate thickness, D_T. Finally, exit velocity V has been normalize by the impact velocity, V_0. In each case the measurements are within 90% of the AUTODYN simulation.

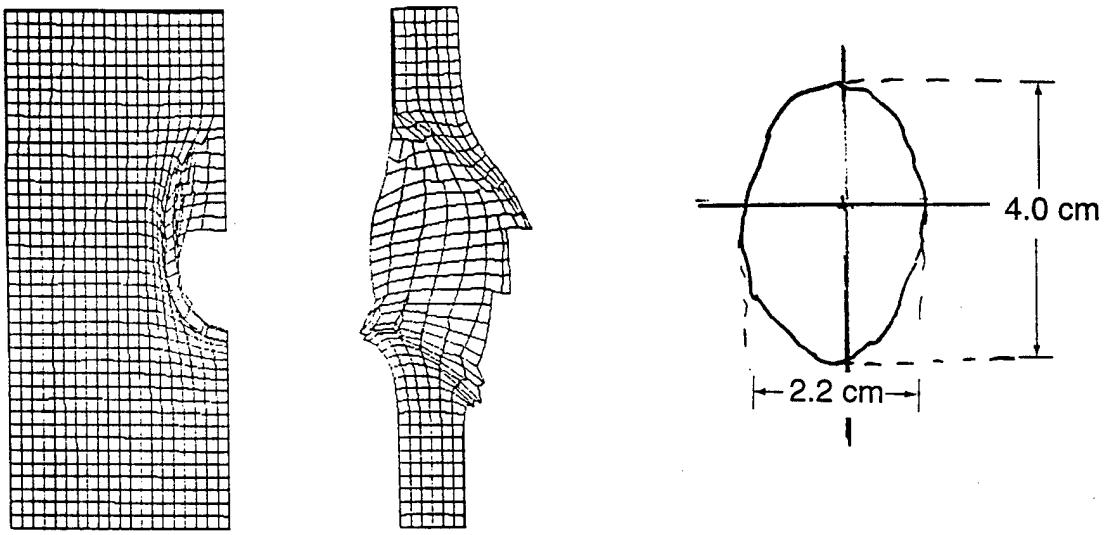

(a)

Measurement		# 240	AUTODYN
Entrance crater	D_{maj}/D_p	5	4.67
	D_{min}/D_p	2.89	2.67
Erosion	E/D_T	2.24	2.5
Velocity	V/V_0	$\sim .96$	$\sim .99$

(b)

Fig. 2. Trace of crater for (a) IAT experiments #240 and (b) comparison with AUTODYN simulation results.

Because a majority of the simulations comprising this study were with relatively coarse cell size, we carried out a simulation using a finer grid size. Figure 3 is an illustration of the differences between the two cell densities, one with four cells across the rod diameter Figure (a) and the second Figure (b) with six cells across the rod diameter. The "snapshots" were made at roughly the same time after initial impact in order to facilitate comparison of distinguishing features.[1] We have previously noted that as the rod penetrates the plate, the penetration channel grows from the initially quasi-spherical impact crater. This can be seen in Figure 3(a) and seen somewhat better in Figure 3(b). The decrease in the cell size appears to improve resolution of the crater shape. However, the simulations are qualitatively very similar. In particular, depth of penetration and crater dimensions appear roughly the same. From this comparison we have concluded that increasing cell size does not appreciably affect the simulation, at least to the accuracy we are interested.

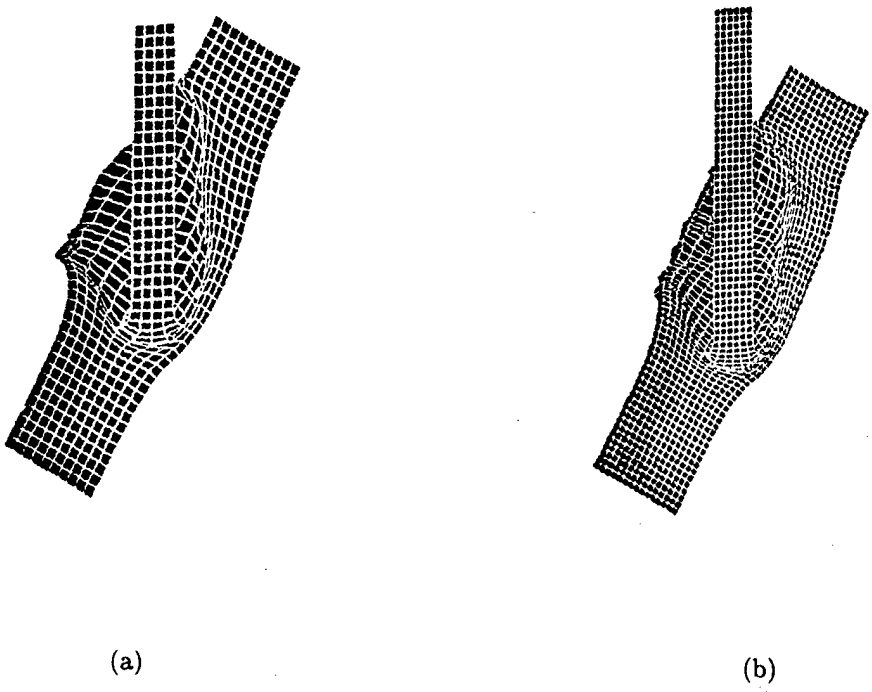

Fig. 3. Oblique penetration simulations of a long rod in RHA steel using two mesh sizes: (a) four cells per diameter.

1. Time is, of course, measured from the beginning of the simulation. Initial conditions were made the same as much as possible. However slight differences exist because of the different mesh sizes. Consequently, run times differed slightly.

The two exercises just described indicate that we are using reasonable grid sizes and the AUTODYN simulations are yielding results which we can reasonably expect to agree with experiments. While these calibrations are not as extensive as we would like, they indicate that we are not making any obvious errors.

Nose shapes and oblique penetration

We have simulated a variety of nose shapes and the resulting craters for oblique impacts and have found that they can achieve a mass saving while maintaining adequate crater dimensions. In general, we have investigated reverse tapered noses in the sense that the lead end or tip is as large or larger that the unmodified rod. In most cases we have seen crater sizes which can easily accommodate the follow-on rod.

Figure 4 shows a comparison of the baseline rod and resulting crater with the exiting portion of the projectile (Figure 4(a)) and one of the most efficient modified nose rods with the resulting crater and exiting residual rod (Figure 4(b)). Note that the crater for the modified rod is significantly smaller than the baseline case, particularly at the crater exit. Nevertheless, the follow-on rod has no difficulty transiting the crater. Furthermore, the residual rod in the modified case is at least as big in the baseline case. Therefore, measured in terms of loss of mass from erosion, the modified rod can be considered a better penetrator.

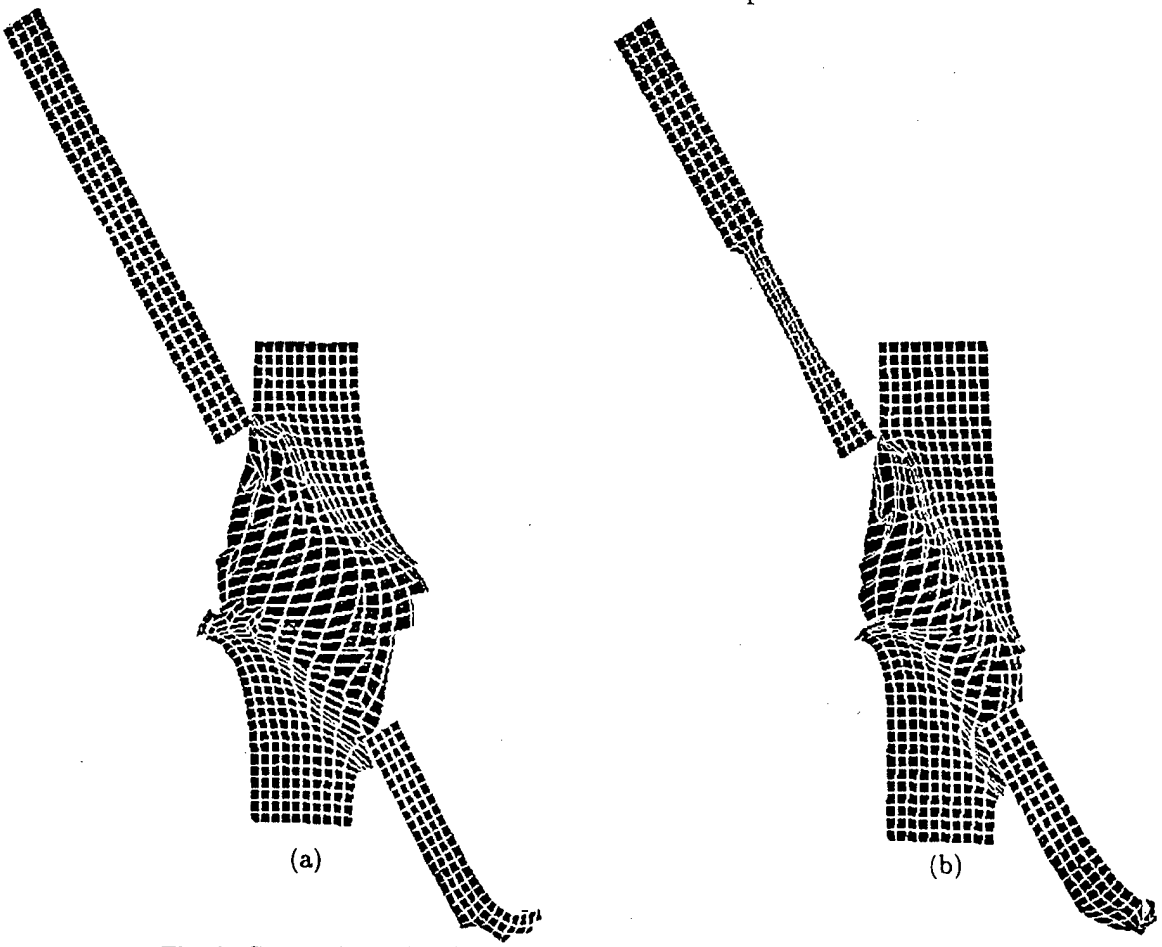

Fig. 4. Comparison of oblique impacts: (a) baseline rod and (b) modified rod.

For the modified case, the mass savings is about 30% for an L/D=10 rod. This percentage will change, of course, for longer rods. However, if we compare the saved mass to the eroded length (say, for example, five diameters) the savings is 60% and this number is independent of the length of the rod. Seen in this light, the mass saved with these types of penetrators is significant. Because of the dramatic success of these penetrators, we were led to explore whether similar results could be achieved in yawed penetration problems.

Yawed oblique impact: general

From our analysis of unyawed oblique impact we expected some gains in using modified penetrator noses for yawed oblique penetrators. However, as noted earlier, yawed impact craters are distinctive in that, in addition to the relatively spherical crater produced by the initial impact, they possess an adjoining narrower slot, or tail giving the crater a keyhole shape (Figure 5). The generation of the slot produces reaction forces on the penetrator, which causes deflection. If the force varies along the rod length, the result will be penetrator distortion.

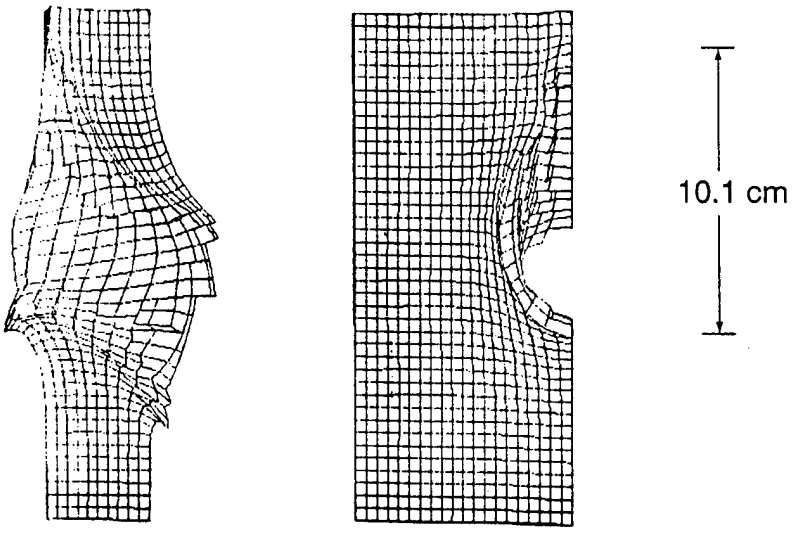

Fig. 5. Keyhole shaped crater for pitch up (nose tipped away from plate) oblique impact.

In unyawed impacts the axis of the projectile is aligned with the velocity vector. In contrast, in yawed impacts the projectile is misaligned and an angle, the yaw angle, exists between the velocity vector and the projectile axis. The yawed oblique impact which created the crater in Figure 5 is illustrated in Figure 6. Note that in yawed impact problems there can be two orientations, one where the rod axis is pitched (yawed) toward the plate (θ and α have opposite signs) and another where the rod is pitched, away from the plate (θ and α have the same sign). The first orientation is considered pitch down and the second pitch up. In each case the penetration process, including the rod damage and crater development, is unique. In ERA nomenclature, the first case represents rear plate interaction and the second case, front plate interaction.

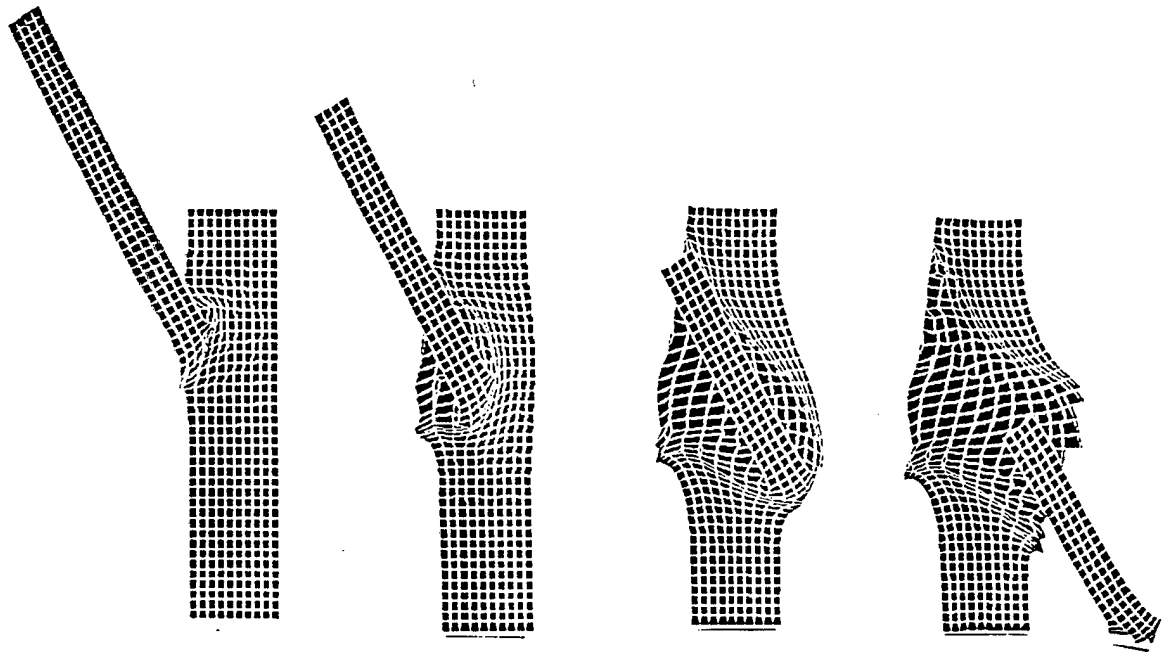

(a)

tungsten	L/D	10
rod	$V_{\parallel}$(km/s)	2.749
	$V_{\perp}$(km/s)	0.270
RHA steel	T/D	1.2
plate	obliquity	60°

(b)

Fig. 6. Positive yawed (nose tipped toward plate) oblique impact (a) sequence of four snapshots for and (b) table of input parameters.

Figure 6 depicts four intervals during a yawed oblique (pitch up) impact of a tungsten rod onto a RHA steel plate (see Table 1). As in the unyawed oblique case, impact initiates a relatively spherical cavitation-generated crater (Figure 6, second panel). Thereafter, the rod tip overtakes the spreading crater surface and begins to preferentially penetrate one side of the crater wall (Figure 6, second panel). Again, this portion of the process is similar to unyawed oblique impacts. However, in contrast to the unyawed oblique impact problem, the upstream rod sidewall comes in contact with the lip of the crater. The crater created by cavitation becomes the hole portion of the keyhole, while the portion of the crater created from sidewall contact becomes the slot portion of the keyhole.

We can see that the rod sidewall will come in contact with the crater lip by noting the yawed rod has a velocity vector with two components, one along the rod axis and another component normal to the axis (radial). The radial component of the rod's velocity vector carries the sidewall toward the crater lip. Because the radial component of velocity is much smaller than the axial component, the slot develops gradually. In fact, in contrast to the crater formed by cavitation, the rod side wall "cuts" into the plate. The process is analogous to a punch or indentation. The slot cutting continues as long as the rod is engaged with the plate and results in the slot portion of the keyhole crater in Figure 5.

While the width of the minor axis across the largest part of the crater in Figure 5 is roughly the same as that for the unyawed case, the length along the major axis of the crater is significantly greater than that in the unyawed case. The greater size of the crater brought about by slot formation results in an additional load on the rod and is applied in a particularly vulnerable portion of the rod, the rod sidewall.

The additional load suffered by the rod as a result of yaw severely alters and deforms the interacting rod because the load is nonuniformly applied and acts along the sidewall. It begins as a point load as the rod initially contacts the crater but broadens as the slot forms so that region of interaction increases throughout penetration. This uneven load can cause rotation and bending of the rod. Second, the interacting sidewall slides along the slot as it cuts into the plate which causes the rod surface to become severely deformed. As a result, in addition to the type of erosion suffered by unyawed projectiles, the yawed projectile is bent and has a severely deformed sidewall. The resulting exiting projectile is not nearly as effective as the unyawed projectile. Despite the deleterious consequences of yawed impacts, we can still expect some positive gains resulting from modified nose shapes.

As we have seen, the rod velocity for yawed oblique impacts has normal and axial components which naturally divide crater formation into two distinct parts. First, axial penetration is the result of the axial velocity of the rod and is similar in many respects to simple oblique penetration. Second, slot cutting is the result of the transverse component of the rod velocity and is not found to occur in unyawed oblique impacts. Defined in this way, axial penetration and slot cutting can be seen to propagate in orthogonal directions. Moreover, simple oblique penetration can be thought of as a special case of yawed oblique impact where the rod has axial velocity and zero normal velocity. Hence, in yawed oblique penetration we expect to see the sort of gains (less mass used to create the key portion of the keyhole crater) we have seen in unyawed oblique impacts from nose shapes in the axial penetration direction and we expect them to be somewhat independent of slot cutting.

Figure 7 shows the impact of a tungsten rod with a modified nose onto a RHA steel plate. We can see the general features of the resulting crater and the loading on the rod sidewall as a result of slot cutting. Note that the crater that appears is more narrow than one would expect for an unyawed rod. This is consistent with the notion that nose shapes should primarily affect axial penetration. Furthermore, it appears that sidewall loading is uniformly distributed along the rod sidewall. The results of the calculation show that uniform loading began almost immediately at initial contact thus avoiding the initial point load of the crater lip. If this is the case then the effect on the rod would be a simple translation rather than rotation or bending.

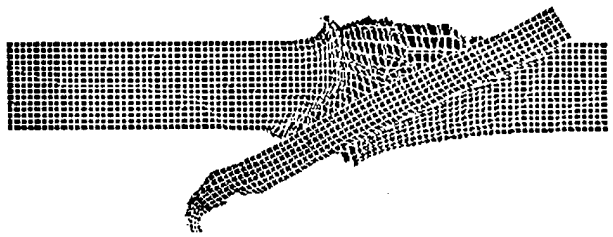

Fig. 7. Positive yaw impact for modified nose projectile.

Summary

We have investigated the effects of nose shapes on simple oblique and yawed oblique impacts. For simple oblique penetration there is a significant amount of rod tip erosion. Novel shaped noses can be designed which minimize the amount of mass lost in erosion and which create efficient craters sufficient to allow passage of the upstream portion of the rod. Gains brought about by novel rod tip designs are not as evident in the yawed oblique impact case as in the simple oblique impact case. The gains made in the axial direction are obscured somewhat by the additional loading due to slot formation. However, nose shapes seem to affect the degree and nature of this load and may provide a means of reducing the damage caused by slot formation.

Acknowledgment

Discussions with Michael Normandia were very helpful in developing the interpretations of slot cutting.

This work was supported by the U.S. Army Research Laboratory (ARL) under contract DAAA21-93-C-0101.

Distribution List

Administrator
Defense Technical Information Center
Attn: DTIC-DDA
8725 John J. Kingman Road,
Ste 0944
Ft. Belvoir, VA 22060-6218

Director
US Army Research Lab
ATTN: AMSRL OP SD TA
2800 Powder Mill Road
Adelphi, MD 20783-1145

Director
US Army Research Lab
ATTN: AMSRL OP SD TL
2800 Powder Mill Road
Adelphi, MD 20783-1145

Director
US Army Research Lab
ATTN: AMSRL OP SD TP
2800 Powder Mill Road
Adelphi, MD 20783-1145

Army Research Laboratory
AMSRL-CI-LP
Technical Library 305
Aberdeen Prvg Grd, MD 21005-5066

Stephan Bless
Institute for Advanced Technology
The University of Texas at Austin
4030-2 W. Braker Lane, Suite 200
Austin, TX 78759

William de Rosset
U.S. Army Research Laboratory
Attn: AMSRL-WT-TC
Aberdeen Prvg Grd, MD 21005-5066

Mehmet Erengil
Institute for Advanced Technology
The University of Texas at Austin
4030-2 W. Braker Lane
Austin, TX 78759

W. J. Gillich
U.S. Army Research Laboratory
AMSRL-WT-TA
Aberdeen Prvg Grd, MD 21005-5066

Tim Holmquist
Alliant Techsystems, Inc.
Twin City Army Ammunition Plant-Bldg. 103
New Brighton, MN 55112

David Littlefield
Institute for Advanced Technology
The University of Texas at Austin
4030-2 W. Braker Lane
Austin, TX 78759

Richard Lloyd
Raytheon
Mail Stop T3TB8
P.O. Box 1201
Tewksburg, MA 01876-0901

Michael Normandia
Institute for Advanced Technology
The University of Texas at Austin
4030-2 W. Braker Lane
Austin, TX 78759

Dennis L. Orphal
International Research Associates
4450 Black Ave. Suite E
Pleasanton, CA 94566

Chadee Persad
Institute for Advanced Technology
The University of Texas at Austin
4030-2 W. Braker Lane
Austin, TX 78759

A. M. Rajendran
US Army Research Lab
AMSRL-MA-PD
Aberdeen PG, MD 21005-5066

Sikhanda Satapathy
Institute for Advanced Technology
The University of Texas at Austin
4030-2 W. Braker Lane
Austin, TX 78759

Graham Silsby
Institute for Advanced Technology
The University of Texas at Austin
4030-2 W. Braker Lane
Austin, TX 78759

Mike Zoltoski
U.S. Army Research Laboratory
Attn: AMSRL-WM-TA
Aberdeen Prvg Grd, MD 21005-5066